

Spectral Type and Geometric Albedo of (98943) 2001 CC21, the *Hayabusa2*# Mission Target

Jooyeon Geem,^{1,2} * Masateru Ishiguro,^{1,2} † Mikael Granvik,^{3,4} Hiroyuki Naito,⁵ Hiroshi Akitaya,^{6,7} Tomohiko Sekiguchi,⁸ Sunao Hasegawa,⁹ Daisuke Kuroda,¹⁰ Tatsuharu Oono,¹¹ Yoonsoo P. Bach,^{1,2} Sunho Jin,^{1,2} Ryo Imazawa,¹² Koji S. Kawabata,⁷ Seiko Takagi,¹³ Makoto Yoshikawa,⁹ Anlaug A. Djupvik,^{14,15} Julie Thiim Gadeberg,¹⁴ Tapio Pursimo,^{14,15} Oliver Durfeldt Pedros,^{14,16} Jeppe Sinkbaek Thomsen,^{14,17} Zuri Gray^{14,18,19}

¹Department of Physics and Astronomy, Seoul National University, 1 Gwanak-ro, Gwanak-gu, Seoul 08826, Republic of Korea

²SNU Astronomy Research Center, Seoul National University, 1 Gwanak-ro, Gwanak-gu, Seoul 08826, Republic of Korea

³Department of Physics, University of Helsinki, P.O. Box 64, FI-00014 Helsinki, Finland

⁴Asteroid Engineering Laboratory, Luleå University of Technology, Box 848, SE-98128 Kiruna, Sweden

⁵Nayoro Observatory, 157-1 Nisshin, Nayoro, Hokkaido 096-0066, Japan

⁶Planetary Exploration Research Center, Chiba Institute of Technology, 2-17-1 Tsudanuma, Narashino, Chiba 275-0016, Japan

⁷Hiroshima Astrophysical Science Center, Hiroshima University, Kagamiyama 1-3-1, Higashi-Hiroshima, Hiroshima 739-8526, Japan

⁸Asahikawa Campus, Hokkaido University of Education, 9 Hokumon, Asahikawa, Hokkaido 070-8621, Japan

⁹Institute of Space and Astronautical Science (ISAS), Japan Aerospace Exploration Agency (JAXA), Sagami-hara, Kanagawa 252-5210, Japan

¹⁰Bisei Spaceguard Center, Japan Spaceguard Association, 1716-3 Okura, Bisei-cho, Ibara, Okayama 714-1411, Japan

¹¹Department of CosmoSciences, Graduate School of Science, Hokkaido University, Kita-ku, Sapporo, Hokkaido 060-0810, Japan

¹²Department of Physics, Graduate School of Advanced Science and Engineering, Hiroshima University Kagamiyama, 1-3-1 Higashi-Hiroshima, Hiroshima 739-8526, Japan

¹³Department of Earth and Planetary Sciences, Faculty of Science, Hokkaido University, Kita-ku, Sapporo, Hokkaido 060-0810, Japan

¹⁴Nordic Optical Telescope, Rambla José Ana Fernández Pérez 7, ES-38711 Breña Baja, Spain

¹⁵Department of Physics and Astronomy, Aarhus University, Ny Munkegade 120, DK-8000 Aarhus C, Denmark

¹⁶DTU Space, National Space Institute, Technical University of Denmark, Elektrovej 328, DK-2800 Kgs. Lyngby, Denmark

¹⁷Dipartimento di Fisica e Astronomia, Università di Bologna, Via Zamboni, 33 - 40126 Bologna, Italia

¹⁸Armagh Observatory and Planetarium, College Hill, Armagh BT61 9DG, UK

¹⁹Mullard Space Science Laboratory, Department of Space & Climate Physics, University College London, Holmbury St. Mary, Dorking, Surrey RH5 6NT, UK

Accepted 20XX. Received 2023; in original form ZZZ

ABSTRACT

We conducted optical polarimetry and near-infrared spectroscopy of JAXA’s *Hayabusa2*# mission target, (98943) 2001 CC21, in early 2023. Our new observations indicated that this asteroid has a polarimetric inversion angle of $\sim 21^\circ$, absorption bands around 0.9 and 1.9 μm , and a geometric albedo of 0.285 ± 0.083 . All these features are consistent with those of S-type but inconsistent with L-type. Based on this evidence, we conclude that JAXA’s *Hayabusa2*# spacecraft will explore an S-type asteroid with albedo and size (0.42–0.56 km when we assume the absolute magnitude of 18.6) similar to (25143) Itokawa.

Key words: minor planets, asteroids: individual: (98943) 2001 CC21 — techniques: polarimetric — techniques: spectroscopic

1 INTRODUCTION

(98943) 2001 CC21 (hereafter CC21) is the target of the *Hayabusa2* extended mission (the nickname is *Hayabusa2*#) operated by the Japan Aerospace Exploration Agency (JAXA). After a successful sample return from (162173) Ryugu in 2020, *Hayabusa2* spacecraft plans to explore its next targets, CC21 in July 2026 and 1998 KY26 in July 2031.

CC21 has a rotation period of 5 hours (Hirabayashi et al. 2021). However, little is known about CC21. Initially, Binzel et al. (2004)

reported that CC21 is classified as L-type. On the contrary, Lazzarin et al. (2005) and DeMeo et al. (2009) pointed out the possibility of an S-complex asteroid (either Sk- or Sw-type). Therefore, the taxonomic type of this space mission target still needs to be examined more thoroughly. In addition, it should be emphasized that CC21’s albedo has yet to be determined. Knowing albedo is critical for setting appropriate exposure times during the *Hayabusa2*#’s fast flyby and estimating the size.

We present our new observational evidence for the taxonomic type and the geometric albedo of this asteroid, taking advantage of the observation opportunity in 2023 January–March. We conducted optical polarimetry in a wide range of phase angles ($\alpha = 21.7^\circ$ – 99.9°), which allows for estimating the taxonomic classification and the

* E-mail: ksky0422@snu.ac.kr

† E-mail: ishiguro@snu.ac.kr

geometric albedo. Moreover, we conducted the near-infrared (NIR, 0.7–2.4 μm) spectroscopy at an intermediate phase angle ($\alpha \sim 32^\circ$). We describe our observations and data reduction in Section 2 and the results in section 3. Based on the results, we discuss our results in section 4.

2 OBSERVATIONS AND DATA ANALYSIS

2.1 Optical Polarimetry

The observation circumstances are summarized in Table 1. We obtained the polarimetric data of CC21 by using three instruments: the FAPOL polarimeter of the Alhambra faint object spectrograph and camera (ALFOSC) on the 2.56-m Nordic Optical Telescope at the Observatorio del Roque de los Muchachos, the Hiroshima optical and near-infrared camera (HONIR; Akitaya et al. 2014) on the 1.5-m Kanata Telescope at the Higashi-Hiroshima observatory and the visible multi-spectral imager (MSI; Watanabe et al. 2012) on the 1.6-m Pirka Telescope at the Nayoro Observatory of Hokkaido University. We employed V- and R-band. All instruments are composed of a rotatable half-wave plate (HWP) and mounted in the Cassegrain focus of each telescope. HONIR and MSI equip a Wollaston prism, and ALFOSC employs a calcite plate mounted in the aperture wheel. To obtain sets of the Stokes parameters, we rotated the HWP in the order of 0° , 45° , 22.5° and 67.5° for HONIR and MSI and from 0° to 337.5° at 22.5° interval for ALFOSC.

The polarimetric data were analyzed in the same manner as described in Ishiguro et al. (2022) for MSI data and in Geem et al. (2022) for ALFOSC and HONIR data. We observed unpolarized standard stars to obtain the instrumental polarization parameters (q_{inst} and u_{inst}) and strongly polarized stars to determine the position angle offset ($\theta_{\text{off}} \equiv \theta_{\text{cat}} - \theta_{\text{obs}}$). Here, θ_{cat} and θ_{obs} are the position angle of a star from a catalog and an observation, respectively. We summarize the instrument calibration parameters in Table 2 and the derived polarimetric degrees in Table 1. In Table 1, the polarization degree with respect to the scattering plane (P_r) is given, as is conventionally driven for asteroid polarimetry. We fit the polarization phase curve (PPC) by using the Lumme–Muinonen function (L/M, Lumme & Muinonen 1993) and the linear function by employing the Markov chain Monte Carlo method implemented in PyMC3 (Salvatier et al. 2016). 10,000 samples per chain with four chains are adopted. We used the same boundary conditions to derive the uncertainties of the optimal parameters written in Geem et al. (2022). The initial guesses of each parameter are $(h, \alpha_0, c_1, c_2) = (0.07 \text{ per cent deg}^{-1}, 20^\circ, 0.1, 0.001)$. Beyond the α_0 , it is known that P_r of intermediate or high-albedo asteroids, such as S-complex asteroids, pseudo-linearly increases with increasing α up to the maximum phase angle (Cellino et al. 2005). Thus, we applied the linear function to derive h and α_0 by using the data at $\alpha < 80^\circ$. The best-fitting results and their uncertainties obtained with the two different fitting functions agree with each other. The results obtained using L/M cover those obtained by the linear fitting. Therefore, we discuss only the results derived from L/M hereafter.

2.2 Near-infrared Spectroscopy

The NIR spectral data (0.7–2.4 μm) were obtained during two nights, 2023 February 5–6 UT, using the SpeX instrument at the Mauna Kea Observatory 3.2-m NASA Infrared Telescope Facility (IRTF). We used the 0.8 arcsec width slit aligned with the parallactic angle (Binzel et al. 2019). We obtained 86 individual asteroidal spectral

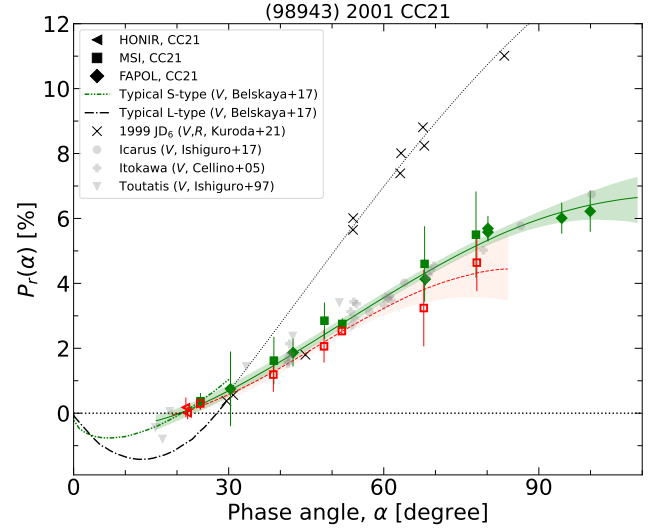


Figure 1. Phase angle (α) dependence of polarization degree (P_r). Data taken by HONIR, MSI, and FAPOL are shown by the triangle, square, and diamond markers, respectively. The filled and empty markers indicate V- and R-bands. The solid and dash lines are curves that fit data in V- and R-bands, respectively, by using the L/M function. The dotted line is the PPC of 1999 JD₆.

images with an integration time of 120s each. The observational circumstances are summarized in Table 3. The standard star of SAO 42382 (G2V) was observed, which is closely located from the asteroid (the airmass difference < 0.1). We used Spextool, an IDL-based spectral reduction program¹ for data reduction (i.e., flat-fielding, sky subtraction, spectrum extraction, and wavelength calibration.).

3 RESULTS

Figure 1 indicates the nightly-averaged PPC. Similar to other asteroids, it shows an upward trend in the observed phase angles, having an inversion angle (α_0) of around 20° and a maximum polarization phase (α_{max}) of around 100° . Table 4 summarizes these key parameters in PPC. For comparison, we plot the typical PPC of the S-type and L-type in low phase angles (Belskaya et al. 2017). We also compare CC21 with S-type asteroids: (1566) Icarus (Ishiguro et al. 2017), (4179) Toutatis (Ishiguro et al. 1997), and (25143) Itokawa (Cellino et al. 2005), in V-band and with an L-type asteroid (85989) 1999 JD₆ in V- and R-bands (Kuroda et al. 2021). A glance at Figure 1 finds that CC21 is closer to these S-type than to the L-type.

It is known that the polarimetric slope h is a good proxy for p_V . The relation between h and p_V is given by $\log_{10}(p_V) = C_1 \log_{10}(h) + C_2$, where C_1 and C_2 are constants (Geake & Dollfus 1986). We derived the p_V by substituting $h = 0.07 \pm 0.02 \text{ per cent deg}^{-1}$ in V-band and obtained $p_V = 0.285 \pm 0.083$ and $p_V = 0.284 \pm 0.076$ using C_1 and C_2 values in Lupishko (2018) and Cellino et al. (2015) (for $p_V > 0.08$), respectively. Although these two albedo estimates are very close, we will henceforth use the former value ($p_V = 0.285 \pm 0.083$), which has the larger error, for safety.

We created α_0 - h plot to discriminate the polarization properties of L-, S-, and other types of asteroids using databases in Kuroda

¹ http://irtfweb.ifa.hawaii.edu/research/dr_resources/

Table 1. Summary of Polarimetry

Date in UT ^a	Inst ^b	Filter	Exp ^c (s)	N ^d	r^e (au)	Δ^f (au)	ϕ^g (°)	α^h (°)	P^i (%)	σP^j (%)	θ_P^k (°)	$\sigma \theta_P^l$ (°)	P_r^m (%)	θ_r^n (°)
Jan 24 18:35–18:49	HONIR	R	60	12	1.14	0.17	213.0	21.7	0.38	0.30	83.7	22.1	0.18	-31.3
Jan 25 17:40–18:00	HONIR	R	60	16	1.14	0.17	208.5	22.1	0.00	0.19	31.7	52.0	-0.00	45.2
Jan 29 14:35–15:14	MSI	R	120	20	1.13	0.16	191.2	24.5	0.31	0.19	-85.0	17.3	0.30	-8.1
Jan 29 15:34–16:45	MSI	V	150	20	1.13	0.16	190.9	24.5	0.45	0.25	-89.8	16.2	0.37	-16.7
Feb 03 23:01–23:10	FAPOL	V	120	8	1.11	0.15	170.3	30.4	1.25	1.15	54.4	26.3	0.75	-26.6
Feb 09 13:39–16:18	MSI	R	120	16	1.09	0.14	151.5	38.6	1.22	0.53	63.5	12.4	1.19	-6.8
Feb 09 16:32–16:50	MSI	V	180	8	1.09	0.14	151.3	38.7	1.62	0.73	73.5	12.9	1.62	-2.8
Feb 11 23:30–23:47	FAPOL	V	120	12	1.09	0.14	144.3	42.4	1.89	0.43	49.8	6.4	1.87	-4.5
Feb 15 13:05–13:28	MSI	R	90	8	1.07	0.14	133.4	48.4	2.09	0.50	45.8	6.9	2.06	-5.2
Feb 15 13:55–14:29	MSI	V	120,240	12,4	1.07	0.14	133.3	48.5	2.92	0.56	35.9	5.5	2.85	6.0
Feb 17 12:03–14:52	MSI	R	90,120	32,24	1.07	0.14	127.4	51.9	2.53	0.12	38.0	1.4	2.53	0.9
Feb 17 13:06–16:08	MSI	V	90,120,150	4,24,24	1.07	0.14	127.2	52.0	2.76	0.17	36.9	1.8	2.75	-1.8
Feb 26 20:42–20:59	FAPOL	V	120	12	1.03	0.13	100.1	68.0	4.13	0.19	8.8	1.3	4.13	-1.3
Feb 26 16:40–16:53	MSI	R	180	8	1.03	0.13	100.5	67.7	3.28	1.18	5.5	10.3	3.24	-4.7
Feb 26 18:28–19:28	MSI	V	240	12	1.03	0.13	100.3	67.9	4.61	1.16	22.4	7.2	4.60	-0.9
Mar 04 14:15–15:20	MSI	R	180	16	1.01	0.13	84.6	78.0	4.66	0.88	8.4	5.4	4.64	-2.5
Mar 04 11:56–13:48	MSI	V	180	20	1.01	0.13	84.9	77.8	5.51	1.33	-6.5	6.9	5.50	1.7
Mar 05 20:35–20:43	FAPOL	V	120	16	1.01	0.13	81.5	80.2	5.69	0.39	-7.7	2.0	5.69	0.8
Mar 13 21:07–21:07	FAPOL	V	120	4	0.98	0.13	62.6	94.4	6.02	0.48	-27.8	2.3	6.01	-0.5
Mar 16 20:24–20:41	FAPOL	V	120	12	0.96	0.13	56.1	99.9	6.33	0.63	-33.5	2.9	6.22	-5.4

^a UT at exposure start, ^b Instrument, ^c Exposure time, ^d Number of valid images, ^e Median heliocentric distance, ^f Median geocentric distance, ^g Position angle of the scattering plane, ^h Median solar phase angle, ⁱ Nightly averaged polarization degree, ^j Uncertainty of P , ^k Position angle of the strongest electric vector, ^l Uncertainty of θ_P , ^m Polarization degree referring to the scattering plane, ⁿ Position angle referring to the scattering plane.

The web-based JPL Horizon system (<http://ssd.jpl.nasa.gov/?horizons>) was used to obtain r , Δ , ϕ , and α in the table.

Table 2. Calibration Parameters of Polarimetry

Inst	Filter	P_{eff}^a (%)	q_{inst} (%)	u_{inst} (%)	θ_{off} (°)	UP ^b	SP ^c	Ref ^d
HONIR	R	97.58	0.010 ± 0.050	-0.008 ± 0.037	38.00 ± 0.83	G191B2B	HD 29333, HD 251204	(1),(2)
ALFOSC	V	100 (assumed)	0.012 ± 0.065	-0.054 ± 0.055	-87.78 ± 0.10	HD 42182, HD 65629	BD+59 389	(3)
MSI	V	99.59 ± 0.02	0.785 ± 0.020	1.077 ± 0.019	-20.61 ± 0.26	HD 15318	HD 7927	(4)
	R	99.55 ± 0.01	0.584 ± 0.011	0.751 ± 0.011	-17.09 ± 0.52	HD 15318	HD 7927	(4)

^a the polarization efficiency, ^b Unpolarized standard stars, ^c Strongly polarized standard stars, ^d the references of standard stars

(1) Turnshek et al. (1990), (2) Whittet et al. (1992), (3) Schmidt et al. (1992), (4) Wolff et al. (1996)

Table 3. Observation Circumstance of Spectroscopy

Date in UT ^a	Exp (s)	α^b (°)	Airmass	N ^c	Solar Analog
Feb 05 09:48–12:39	120	32.3	1.18–1.41	38	SAO 42382
Feb 06 06:08–09:38	120	33.7	1.20–1.69	48	SAO 42382

^a UT at exposure start, ^b solar phase angle, ^c number of valid images

Table 4. PPC Fitting Result

Filter	slope h (% deg ⁻¹)	α_0 (°)	P_{max} (%)	α_{max} (°)
V	0.07 ^{+0.02} _{-0.02}	20.7 ^{+3.3} _{-2.6}	6.7 ^{+1.0} _{-0.6}	114.5 ^{+5.4} _{-12.2}
R	0.06 ^{+0.01} _{-0.02}	21.2 ^{+2.2} _{-2.2}	4.3 ^{+3.5} _{-1.2}	88.4 ^{+31.5} _{-8.4}

et al. (2021) and Lupishko (2022) (Figure 2). Because h and p_V are inversely correlated, asteroids with lower p_V are typically found higher up in the plot. L-type asteroids are known to have distinctively larger α_0 than other asteroids. From this comparison, α_0 - h of CC21 matches those of S-types rather than L-types.

The NIR spectra obtained over the two nights are consistent with each other. No rotational variation of the target spectra is found during the observations. For this reason, we combined all spectral data from two nights. Figure 3 shows the resultant spectrum. The plot

compares CC21's reflectance spectrum with typical S- and L-type asteroids from DeMeo et al. (2009). Our CC21 spectrum indicates not only the clear absorption around 0.9 μm but also the shallow absorption around 1.9 μm associated with pyroxene. The continuum in the visible range at 0.75 μm is confirmed. These features are characteristic of S-type asteroids and are not found in L-type.

4 DISCUSSION

In the previous studies, CC21 was classified in either L- or S-type (Binzel et al. 2004; Lazzarin et al. 2005; DeMeo et al. 2009). Our observations indicates S-type features and rules out L-type possibility. Although empirical, L-type asteroids are known to have distinctive α_0 values compared to other asteroids. The α_0 value in this study is predominantly different from that of L-type asteroids but is consistent with S-type asteroids. Another important aspect of our polarimetry is that the geometric albedo was determined. The derived CC21's albedo ($p_V = 0.285 \pm 0.083$) is in the range of S-type asteroids ($p_V = 0.258 \pm 0.087$, DeMeo & Carry 2013) but is slightly higher than the average L-type asteroids ($p_V = 0.183 \pm 0.089$, DeMeo & Carry 2013). We also emphasize that our NIR spectrum with a good S/N provides definitive evidence for the taxonomic type. Our NIR spectrum agrees with the previous CC21's NIR spectra (Lazzarin

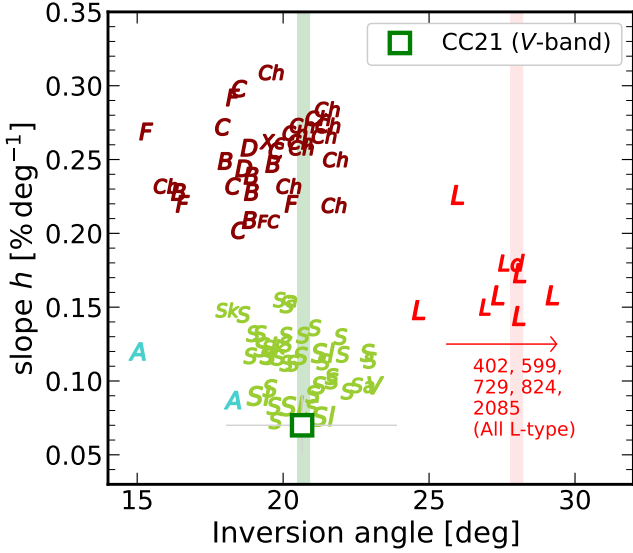


Figure 2. A comparison with other types of asteroids (Kuroda et al. 2021; Lupishko 2022). Each marker indicates the taxonomic type of asteroid (Tholen or Bus–DeMeo type). CC21 in V-band is shown as the green empty box. L-type asteroids with $\alpha_0 \geq 25^\circ$ and unknown h are shown below the arrow (Lupishko 2022). The green and red colored boxes show the typical α_0 ranges of the S-type and the L-type, respectively, from Belskaya et al. (2017).

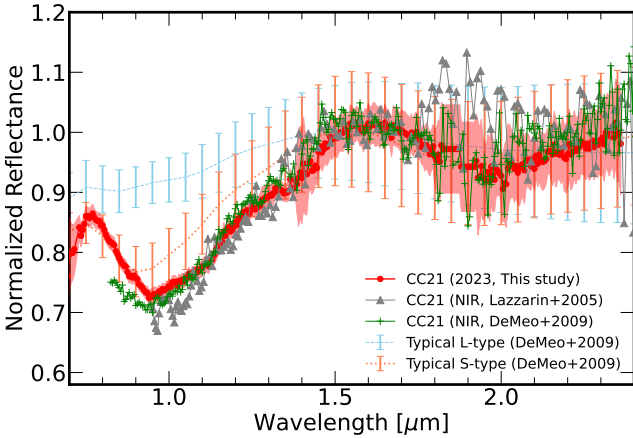


Figure 3. The combined spectra of CC21 from two nights' observations is colored red. For the comparison, NIR spectra of CC21 from the previous studies (Lazzarin et al. 2005; DeMeo et al. 2009) by the gray triangle, green cross markets. The coral dotted and blue dashed lines show the typical spectra of S-type and L-type asteroids (DeMeo et al. 2009), respectively. The reflectances are normalized at $1.6 \mu\text{m}$.

et al. 2005; DeMeo et al. 2009) within observational uncertainty (Marsset et al. 2020) (Figure 3). The 0.9 and $1.9 \mu\text{m}$ absorption features (typical of S-type) are detected. Using an online-based classification tool², CC21 is further subcategorized into Sq or Q-type. These taxonomic types (less weathered ordinary chondritic asteroids) are common in the near-Earth region. Given all these observational results, we conclude that CC21 is an S-type rather than L-type. We

² <http://smass.mit.edu/cgi-bin/busdemeoclass.cgi>

expect that a discussion of the scientific case of *Hayabusa2#* will be conducted with the S-type in consideration.

The second significant point of our study is to determine the albedo. Because *Hayabusa2#* will conduct a fast flyby with CC21, the exposure times should be pre-determined based on the geometric albedo and scattering phase function. The geometric albedo of an S-type asteroid, (25143) Itokawa, was estimated by polarimetry before the launch (Cellino et al. 2005). Notably, the geometric albedo estimated by the polarization method matches the actual value derived by the in-situ observation (Lee & Ishiguro 2018; Tatsumi et al. 2018). Considering that CC21 is an S-type asteroid, our albedo value obtained by the same method as Cellino et al. (2005) is also quite reliable. Our albedo estimate is higher than the assumed value in Hirabayashi et al. (2021) ($p_V = 0.15$). Although we need to refer to the absolute magnitude $H_V = 18.6$ from the literature (Binzel et al. 2004), the effective diameter of CC21 estimated from our albedo would be 0.42–0.56 km. Note that the size becomes smaller than the value in the previous research Hirabayashi et al. (2021).

Polarimetry at large phase angles is also useful for estimating particle size on the asteroid's surface. It is known that the P_{\max} is correlated with the p_V and the grain size. Their relationship is given by $d = 0.03 \exp(2.9(\log(10^2 A) + 0.845 \log(10 P_{\max})))$, where d is the grain size in μm and A is an albedo at $\alpha = 5^\circ$ (Shkuratov & Opanasenko 1992). We calculate CC21's $A = 0.198 \pm 0.058$ by considering the intensity ratio of $I(0^\circ.3)/I(5^\circ) = 1.44 \pm 0.04$ for typical S-type asteroids (Belskaya & Shevchenko 2000). As a result, CC21 would be covered by grain with the size of 100–130 μm , like (1566) Icarus, another near-Earth S-type asteroid whose size is similar to CC21 ($\lesssim 1 \text{ km}$).

5 SUMMARY

We conducted optical polarimetric and near-infrared spectroscopic observations of 2001 CC21 in early 2023. The inversion angle ($\alpha_0 \sim 21^\circ$) and geometric albedo ($p_V \sim 0.3$) are consistent with those of S-types but significantly different from those of L-types. The near-infrared spectrum of the target shows clear absorption bands around 0.9 and $1.9 \mu\text{m}$, which are the typical spectral features of S-type asteroids. Based on the results, we conclude that 2001 CC21 is a near-Earth S-type asteroid with an albedo of $p_V = 0.285 \pm 0.083$ and a size of 0.42–0.56 km.

ACKNOWLEDGEMENTS

This research at SNU was supported by a National Research Foundation of Korea (NRF) grant funded by the Korean government (MEST) (No. 2023R1A2C1006180). SH was supported by the Hypervelocity Impact Facility (former name: The Space Plasma Laboratory), ISAS, JAXA. The data presented here were obtained with ALFOSC, which is provided by the Instituto de Astrofísica de Andalucía (IAA) under a joint agreement with the University of Copenhagen and NOT. Based on observations made with the Nordic Optical Telescope, owned in collaboration by the University of Turku and Aarhus University, and operated jointly by Aarhus University, the University of Turku and the University of Oslo, representing Denmark, Finland and Norway, the University of Iceland and Stockholm University at the Observatorio del Roque de los Muchachos, La Palma, Spain, of the Instituto de Astrofísica de Canarias.

DATA AVAILABILITY

The observational data are available in Zenodo³. The source codes and scripts for the data analyses, plots, and resultant data tables are available via the GitHub service⁴.

REFERENCES

- Akitaya H., et al., 2014, *Proc. SPIE*, 9147, 914740
 Belskaya I. N., Shevchenko V. G., 2000, *Icarus*, 147, 94
 Belskaya I. N., et al., 2017, *Icarus*, 284, 30
 Binzel R. P., Perozzi E., Rivkin A. S., Rossi A., Harris A. W., Bus S. J., Valsecchi G. B., Slivan S. M., 2004, *M&PS*, 39, 351
 Binzel R. P., et al., 2019, *Icarus*, 324, 41
 Cellino A., Yoshida F., Anderlucci E., Bendjoya P., Di Martino M., Ishiguro M., Nakamura A. M., Saito J., 2005, *Icarus*, 179, 297
 Cellino A., Bagnulo S., Gil-Hutton R., Tanga P., Cañada-Assandri M., Tedesco E. F., 2015, *MNRAS*, 451, 3473
 DeMeo F. E., Carry B., 2013, *Icarus*, 226, 723
 DeMeo F. E., Binzel R. P., Slivan S. M., Bus S. J., 2009, *Icarus*, 202, 160
 Geake J. E., Dollfus A., 1986, *MNRAS*, 218, 75
 Geem J., et al., 2022, *MNRAS*, 516, L53
 Hirabayashi M., et al., 2021, *Advances in Space Research*, 68, 1533
 Ishiguro M., Nakayama H., Kogachi M., Mukai T., Nakamura R., Hirata R., Okazaki A., 1997, *PASJ*, 49, L31
 Ishiguro M., et al., 2017, *AJ*, 154, 180
 Ishiguro M., et al., 2022, *MNRAS*, 509, 4128
 Kuroda D., Ishiguro M., Naito H., Watanabe M., Hasegawa S., Takagi S., Kuramoto K., 2021, *A&A*, 646, A51
 Lazzarin M., Marchi S., Magrin S., Licandro J., 2005, *Monthly Notices of the Royal Astronomical Society*, 359, 1575
 Lee M., Ishiguro M., 2018, *A&A*, 616, A178
 Lumme K., Muinonen K., 1993, *IAU Symp.160: Asteroids, Comets, Meteors 1993*, 160, 194
 Lupishko D. F., 2018, *Solar System Research*, 52, 98
 Lupishko D., 2022, *NASA Planetary Data System*, p. 1
 Marsset M., et al., 2020, *The Astrophysical Journal Supplement Series*, 247, 73
 Salvatier J., Wieckiâ T. V., Fonnesbeck C., 2016, *Astrophysics Source Code Library*, record ascl:1610.016
 Schmidt G. D., Elston R., Lupie O. L., 1992, *AJ*, 104, 1563
 Shkuratov I. G., Opanasenko N. V., 1992, *Icarus*, 99, 468
 Tatsumi E., et al., 2018, *Icarus*, 311, 175
 Turnshek D. A., Bohlín R. C., Williamson R. L. I., Lupie O. L., Koornneef J., Morgan D. H., 1990, *AJ*, 99, 1243
 Watanabe M., Takahashi Y., Sato M., Watanabe S., Fukuhara T., Hamamoto K., Ozaki A., 2012, in *Ground-based and Airborne Instrumentation for Astronomy IV*, p. 84462O, doi:10.1117/12.925292
 Whittet D. C. B., Martin P. G., Hough J. H., Rouse M. F., Bailey J. A., Axon D. J., 1992, *ApJ*, 386, 562
 Wolff M. J., Nordsieck K. H., Nook M. A., 1996, *AJ*, 111, 856

This paper has been typeset from a $\text{\TeX}/\text{\LaTeX}$ file prepared by the author.

³ <https://doi.org/10.5281/zenodo.XXXXX>

⁴ <https://github.com/Geemjy/XXXXX.git>